NUMERICAL ANALYSIS OF THE DEVELOPMENT OF A SYSTEM OF JETS IN THE REGION OF MIXING OF OPPOSITELY TWISTED ANNULAR FLOWS

A. L. Dorfman

UDC 532.516

Results are presented from a study of the flow structure and mass transfer in a combustion chamber employing the microflame diffusion principle of combustion in a twisted flow. The study was conducted with an isothermal computational model.

The interaction of oppositely twisted coaxial jets separated by an annular gap was examined in [1]. It was shown on the basis of numerical solution of turbulent flow equations that the intensity of the recirculation zone beyond the annular gap monotonically decreases with an increase in twist. The scheme of combustion examined here provides for the injection of single-pass jets of a gaseous fuel into the recirculation zone beyond the annular gap separating two oppositely twisted air flows. Here under actual conditions increasing the twist has a positive effect, despite the above-noted decrease in the intensity of the recirculation zone. Increasing the twist stabilizes the combustion process to a certain degree. Since the effectiveness of the diffusion method of combustion is determined primarily by the intensity of heat and mass exchange between the gaseous fuel and air and the combustion products, it is interesting to study the structure of the flow formed as a result of the interaction of a system of single-pass jets and coaxial, oppositely twisted flows and its effect on heat exchange. Although some progress has by now been made in the numerical modeling of flows with combustion [2, 3], this study is limited to the case of isothermal flow. This is primarily because we can expect the aerodynamic structure of the flow to be dynamically similar under isothermal and nonisothermal conditions. Thus, a study conducted in an isothermal approximation can reveal characteristic flow features responsible for intensifying heat and mass transfer and can make it possible to evaluate the effect of different factors on them. Since detailed experimental study of the structure of a three-dimensional flow with combustion in a combustion chamber is difficult due to a number of technical factors, the data obtained in numerical experiments is important for understanding hydrodynamic and heat and mass transfer processes occurring in an actual combustion chamber.

Figure 1a shows the flow examined. An annular surface 1 dividing oppositely twisted flows emanating from swirlers 2 is located at the inlet of an annular channel of height H and mean radius R. A system of single-pass jets is directed from holes of radius r located about the periphery of a surface 1 of radius R with a spacing s between the holes. The surface 1 is located symmetrically heightwise with respect to the annular channel and is characterized by a height h. We are examining the case of small ratios H/R and s/R, which, considering the periodicity of the flow, permit approximation of an annular channel on a period s by a channel formed by two parallel planes. We may further reliably assume that the flow on the period s has symmetrical rotation through 180° relative to the point of discharge of the jet. All this makes it possible to limit ourselves in the numerical analysis to a region in the form of a parallelepiped of height H/2 and width s. The region begins with the surface 1 and extends downstream over a distance $x_M^1 = 4H$.

The system of equations of the mean turbulent flow

$$\frac{\partial v^i}{\partial t} + \frac{\partial}{\partial x^j}(v^i v^j + \tau^{ij} + \delta^{ij} p) = 0; \quad \frac{\partial v^j}{\partial x^j} = 0, \; i, \; j = 1, \; 2, \; 3,$$

is closed by introducing the scalar turbulent viscosity ε, connecting the components of the turbulent-stress tensor with the components of the mean-flow strain-rate tensor. Here, in

"Leningradskii Metallicheskii Zavod" Industrial Association of Turbine Manufacture.
Translated from Inzhenerno-Fizicheskii Zhurnal, Vol. 44, No. 6, pp. 941-949, June, 1983. Original article submitted January 27, 1982.

 0022-0841/83/4406-0636$07.50

the region of the flow occupied by the jet, turbulent viscosity is assumed to be constant and equal to $\varepsilon = cU_c r$, by analogy with a circular turbulent jet [4] (c = 0.01-0.03). To determine turbulent viscosity outside the jet, we used the mixing length formula

$$\varepsilon = L^2 \sqrt{\frac{1}{2}\sum_{i,j=1}^{3}\left(\frac{\partial v^i}{\partial x^j}+\frac{\partial v^j}{\partial x^i}\right)^2}$$

with the distribution of mixing length L from [1], which earlier made it possible to obtain satisfactory agreement between theoretical and experimental distributions of velocity for axisymmetrical flow without jets [1]. The parameters in the expression for mixing length [1] and the value of c agreed so as to ensure agreement of ε on the boundaries of the isolated characteristic flow regions. Here the region to which the values belonged was determined in a numerical calculation on the basis of analysis of the velocity field.

The boundary conditions were as follows:

$$v^1(0,\ x^2,\ x^3) = \begin{cases} U_0, & x^3 > h/2; \\ 0, & x^3 \leqslant h/2,\ \rho > r; \\ U_c, & x^3 \leqslant h/2,\ \rho \leqslant r; \end{cases}$$

$$\rho = \sqrt{(x^3)^2 + (x^2 - s/2)^2};$$

$$v^2(0,\ x^2,\ x^3) = \begin{cases} V_0, & x^3 > h/2; \\ 0, & x^3 \leqslant h/2; \end{cases}$$

$$v^3(0,\ x^2,\ x^3) = 0;\ v^k(x^1,\ x^2,\ H/2) = 0,\ k = 1,\ 2,\ 3;$$

$$\frac{\partial v^k}{\partial x^3}(x^1,\ x^2,\ 0) = -\frac{\partial v^k}{\partial x^3}(x^1,\ s - x^2,\ 0),\ k = 1,\ 2;$$

$$v^3(x^1,\ x^2,\ 0) = -v^3(x^1,\ s - x^2,\ 0);$$

$$v^k(x^1,\ 0,\ x^3) = v^k(x^1,\ s,\ x^3),\ k = 1,\ 2,\ 3;$$

$$\frac{\partial}{\partial x^1}\frac{\partial v^1}{\partial x^1}(x^1_M,\ x^2,\ x^3) = 0;\ \frac{\partial v^k}{\partial x^1}(x^1_M,\ x^2,\ x^3) = 0,\ k = 2,\ 3.$$

Together with calculation of the characteristics of motion, we studied mass transfer by solving the transport equation for the substance γ:

$$\frac{\partial \gamma}{\partial t} + \frac{\partial}{\partial x^i}(\gamma v^i + q^i) = 0.$$

The coefficient of turbulent diffusion, connecting q_j with $\partial\gamma/\partial x^j$, was expressed through the eddy viscosity with a diffusional Prandtl number equal to 0.7. For boundary conditions we used homogeneous Neumann conditions on impermeable surfaces: $\gamma = 0$ at the swirler outlet, $\gamma = \gamma_c$ at the mouth of the jet, and $\partial/\partial x^1(\partial\gamma/\partial x^1) = 0$ at the downstream boundary.

The flow and mass transfer patterns obtained from the calculations were compared with data from visual observations and measurements of the flow on an experimental stand. The scalar substance was modeled in the experiment by slight initial heating of the jet relative to the main flow, with subsequent temperature measurement.

The problem posed was solved in two stages. In the first stage we found the solution corresponding to steady-state flow in the investigated region. We then solved the transport equation for the scalar substance until we reached the corresponding value, here using the velocity field that was found. We increased the accuracy of the finite-difference solution by using the coordinate transformation $\xi^i = \xi^i(x^i)$ in the initial system of equations so that, in selecting constants throughout the region of integration of the grid intervals $\Delta\xi^i$, we reduced the intervals Δx^i near the solid boundaries and in the region occupied by the jet. This transformation has the form

$$\xi^i = \xi^i_0 + \operatorname{sgn}(x^i - x^i_0)\ln(1 + \alpha^i |x^i - x^i_0|),$$

where

$$x_0^1 = \xi_0^1 = 0;\ x_0^2 = s/2;\ \xi_0^2 = \ln(1 + \alpha^2\ s/2);$$

$$x_0^3 = \begin{cases} 0, & 0 \leqslant x^3 \leqslant H/4; \\ H/2, & H/4 < x^3 \leqslant H/2; \end{cases} \quad \xi_0^3 = \begin{cases} 0, & 0 \leqslant x^3 \leqslant H/4: \\ 2\ln(1 + \alpha^3 H/4), & H/4 < x^3 \leqslant H/2, \end{cases}$$

here

$$\frac{\partial}{\partial x^i} = a^i \frac{\partial}{\partial \xi^i},\ a^i = \frac{d\xi^i}{dx^i} = \frac{\alpha^i}{\exp|\xi^i - \xi_0^i|}.$$

To construct the numerical solution we used a uniform three-dimensional grid subdividing the investigated region into a system of elemental cells in the form of a parallelepiped with sides $\Delta\xi^i$. The scalar variables p and γ were determined in the center of the cells, identified by indices (m, l, k). The components of the velocity vector v^i were determined in the center of the corresponding sides of the cell, normal to ξ^i (see Fig. 1b). Henceforth, the subscripts with the variables will indicate their spatial coordinates, i.e., $\varphi_{(m,l,k)} \equiv \varphi(\xi_m^1, \xi_l^2, \xi_k^3)$, $\xi_j^i = (j - 1/2)\Delta\xi^i$, with a half-integral value of the subscript corresponding to a point on the side of the cell. The superscript will denote the number of the time layer or the number of the step in the finite-difference algorithm.

We solved the motion equations using a finite-difference algorithm with a physical division [5-8], characterized by the fact that the transition from known values of the sought functions on the n-th time layer (t = nΔt) to the values on the n+1-st time layer consists of two steps: in the first step we calculate preliminary values of the velocity vector components with allowance for convective accelerations and turbulent flow and without allowance for the continuity equation. The final values of the velocity vector components are obtained in the second step by combining the preliminary values obtained in the first step and terms accounting for the pressure gradient. Here the pressure values should ensure satisfaction of the continuity equation. The first step itself is broken down into three substeps. The first two substeps make allowance for the convective terms of the motion equations by means of an explicit predictor–corrector scheme, this being a modification of McCormick's scheme [9]. The modification consists of allowing for the local orientation of the flow in recording the finite-difference relations, as well as the somewhat different form of the finite-difference record of the flows through the side of the theoretical cell. This is due to the location of the grid functions relative to the latter. The terms accounting for turbulent friction are included in the scheme in the third substep by means of representation through the grid functions from the n-th time layer. The grid variables not determined at some point are found at this point by interpolation using the values at the adjacent points. For example, for v^1 the first step of the finite-difference algorithm has the form (the subscript (m + 1/2, l, k) has been omitted from v^1).

$$v^{1(1)} = v^{1(n)} - \Lambda v^{1(n)};\ v^{1(2)} = \frac{1}{2}(v^{1(n)} + v^{1(1)} - \Lambda v^{1(1)});$$

$$v^{1(3)} = v^{1(2)} - \sum_{j=1}^{3} \lambda^j_{(m+\frac{1}{2},\ l,\ k)}\ \mu^j \tau^{1j}_{(m+\frac{1}{2},\ l,\ k)};$$

$$\Lambda = \lambda^1_{(m+\frac{1}{2},l,k)} \left\{ v^{1(n)}_{(m+1,l,k)}\ \Phi^1_+ - v^{1(n)}_{(m,l,k)}\ \Phi^1_- \right\} + \lambda^2_{(m+\frac{1}{2},l,k)} \left\{ v^{2(n)}_{(m+\frac{1}{2},l+\frac{1}{2},k)}\ \Phi^2_+ - v^{2(n)}_{(m+\frac{1}{2},l-\frac{1}{2},k)}\ \Phi^2_- \right\} +$$

$$+ \lambda^3_{(m+\frac{1}{2},l,k)} \left\{ v^{3(n)}_{(m+\frac{1}{2},l,k+\frac{1}{2})}\ \Phi^3_+ - v^{3(n)}_{(m+\frac{1}{2},l,k-\frac{1}{2})}\ \Phi^3_- \right\};$$

$$\Phi^i_+ = \Theta^i E^i_1 + (1 - \Theta^i) I;\ \Phi^i_- = \Theta^i I + (1 - \Theta^i) E^i_{-1}.$$

The values of Θ^i are determined, on the one hand, by the algorithm by McCormick's method [9] (alternation of the direction of the differences on the predictor and corrector, which provides a second-order approximation) and, on the other hand, by the local orientation of the flow: at the predictor substep $\Theta^i = \delta(v^{i(n)}_{(m+\frac{1}{2},l,k)})$, while at the corrector substep $\Theta^i = 1 - \delta(v^{i(n)}_{(m+\frac{1}{2},l,k)})$, where $\delta(z)$ is an asymmetric unit function equal to 1 with negative z, and 0 in the opposite case. To ensure sequential satisfaction of the predictor and corrector near the

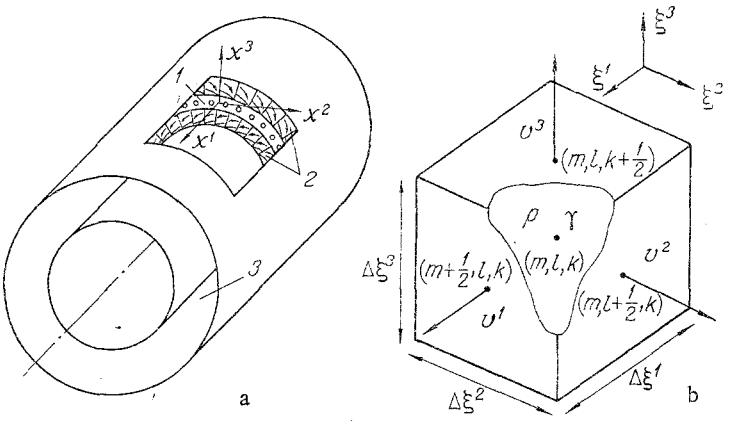

Fig. 1. Flow diagram (a) and theoretical finite-difference cell (b).

boundaries of the region of integration and allow for the boundary conditions, we can determine Θ^i in the opposite manner: $1-\delta(v^{i(n)}_{(m+\frac{1}{2},l,k)})$ on the predictor and $\delta(v^{i(n)}_{(m+\frac{1}{2},l,k)})$ on the corrector. Thanks to allowing for the local orientation of the flow with certain relations between the spatial and time intervals (stability conditions), the region of dependence of the difference scheme will always contain the region of dependence of the differential equations.

We similarly formulate the first step of the finite-difference algorithm for $v^2_{(m,l+\frac{1}{2},k)}$ and $v^3_{(m,l,k+\frac{1}{2})}$. The second step is represented in the form

$$v^{1(n+1)}_{(m+\frac{1}{2},l,k)} = v^{1(3)}_{(m+\frac{1}{2},l,k)} - \lambda^1_{(m+\frac{1}{2},l,k)}\,\Delta^1 p^{(n+1)}_{(m,l,k)};$$

$$v^{2(n+1)}_{(m,l+\frac{1}{2},k)} = v^{2(3)}_{(m,l+\frac{1}{2},k)} - \lambda^2_{(m,l+\frac{1}{2},k)}\,\Delta^2 p^{(n+1)}_{(m,l,k)};$$

$$v^{3(n+1)}_{(m,l,k+\frac{1}{2})} = v^{3(3)}_{(m,l,k+\frac{1}{2})} - \lambda^3_{(m,l,k+\frac{1}{2})}\,\Delta^3 p^{(n+1)}_{(m,l,k)}.$$

Use of a finite-difference representation of the continuity equation

$$v^1_{(m,l,k)}\nabla^1 v^{1(n+1)}_{(m+\frac{1}{2},l,k)} + v^2_{(m,l,k)}\nabla^2 v^{2(n+1)}_{(m,l+\frac{1}{2},k)} + v^3_{(m,l,k)}\nabla^3 v^{3(n+1)}_{(m,l,k+\frac{1}{2})} = 0$$

makes it possible, by insertion of the relations of the second step into it, to obtain a Poisson difference equation for pressure. The boundary conditions here are obtained on the basis of joint inspection of the difference representations of the continuity equation, the boundary conditions of the problem, and the conditions of conservation of total flow rate through the region of integration. For the problem being examined we have: Neumann difference conditions $x^1 = 0$, $x^1 = x^1_M$, $x^2 = H/2$, periodicity conditions for the boundaries $x^2 = 0$ and $x^2 = s$, and the condition of symmetry of rotation relative to a straight line ($x^2 = s/2$; $x^3 = 0$) for the boundary $x^3 = 0$. The equation for pressure was solved on each time layer by the method of optimum upper relaxation. The value of the relaxation coefficient was determined by the number of grid nodes and the parameters of the α_i coordinate transformation and was found to lie within 1.3-1.85. The number of iterations was determined by the accuracy of the satisfaction of the continuity equation, which was systematically evaluated over a specified number of time intervals by calculating in each elemental cell the ratio of the loss of mass of liquid to the total flow through the cell. This value was maintained at 10^{-4}-10^{-5}. It should be noted that, in view of the conservativeness of the finite-difference algorithm, the total loss of mass is equal to zero to within the rounding error.

As the initial conditions we used either the solution of the axisymmetric problem in [1] or data from calculations with approximately the same parameters, making it possible to significantly shorten the time until we reached the steady state. It was determined from the

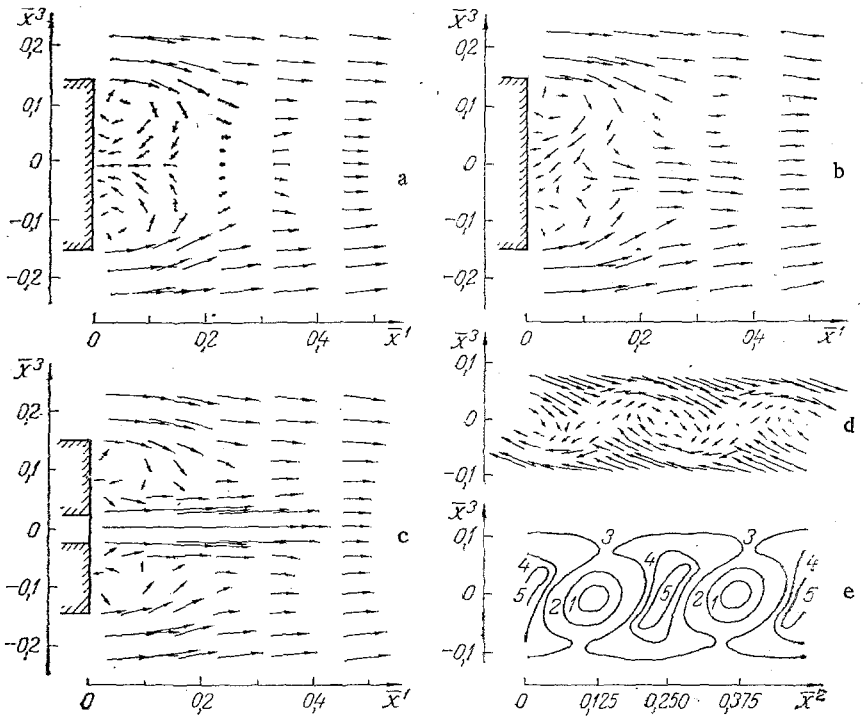

Fig. 2. Flow structure with $\Omega = 60°$, $\Psi = 0.3$, $\varkappa = 4$, $\sigma = 0.83$. Projections of the velocity vectors on the planes: a) $\bar{x}^2 = 0$; b) 0.0625; c) 0.125; d) $\bar{x}^1 = 0.1$; e) lines of equal values of the dimentionless longitudinal coordinate v^1/U_0 in the section $\bar{x}^1 = 0.1$; 1) 2.0; 2) 1.0; 3) 0; 4) −0.2; 5) −0.3.

changes in the flow parameters at characteristic points. The time interval was determined on the basis of local stability conditions obtained from spectral analysis in a linear approximation

$$\Delta t \leqslant \left[\sum_{i=1}^{3} v^i |v^i| + \varepsilon \sum_{i=1}^{3} (v^i)^2\right]^{-1}$$

The algorithm is of the second order of approximation with respect to the spatial variables.

The transport equation was solved using the above-described modified McCormick scheme for the convective terms and representation of the diffusion terms by an explicit scheme. A correction procedure was used to suppress oscillations of γ occurring in the initial intervals in regions with large gradients of γ and leading to the appearance of negative values of low absolute magnitude.

The number of grid nodes for each coordinate and the transform parameters were chosen on the basis of analysis of the effect of scheme factors on flow characteristics (see [1]). A typical finite-difference grid consisted of 8000 nodes. Calculation of the velocity field took 30-60 min, while calculation of mass exchange took 3-10 min of the processor time of the ES-1060 computer.

The following main factors affecting flow characteristics and mass exchange were singled out: the angle of initial twist of the flow from the swirlers $\Omega = \arctan(n)$, $n = V_0/U_0$, the degree of blockage of the annular channel $\Psi = h/H$, the relative discharge velocity of the jet $\varkappa = U_c/U_0$, and the relative distance (spacing) between the jets $\sigma = s/h$. The numerical study was conducted in the following parameter ranges: $0° \leqslant \Omega \leqslant 75°$, $0.2 \leqslant \Psi \leqslant 0.5$, $0 \leqslant \varkappa \leqslant 12$, $0.5 \leqslant \sigma \leqslant 1.5$, and $r/H = 0.025$.

The flow structure can be judged from the typical flow pattern shown in Fig. 2. The zone of longitudinal recirculation beyond the annular surface has a complex three-dimensional shape. The character of the dependence of the relative length of this zone (ratio of the maximum value of the longitudinal coordinate x^1 with zero velocity v^1 to the height of the annular surface) on the parameters Ω and Ψ turned out to be the same as in the case of axisymmet-

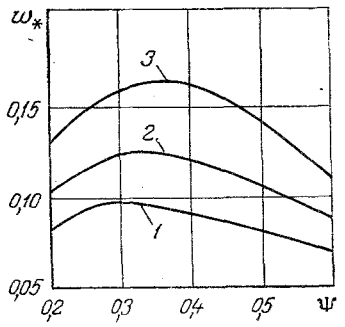

Fig. 3

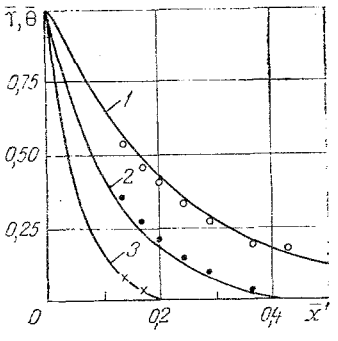

Fig. 4

Fig. 3. Dependence of intensity of transverse circulation on Ω and Ψ with $\varkappa = 4$, $\sigma = 0.83$; 1) Ω = 30°; 2) 45°; 3) 60°.

Fig. 4. Distribution of the scalar substance along the jet axis with Ψ = 0.427 and $\sigma = 1.5$: 1) Ω = 0°, $\varkappa = 2$; 2) Ω = 30°, $\varkappa = 1.3$; 3) Ω = 45°, $\varkappa = 0.8$; points indicate experimental data.

ric flow without jets [1]: an increase in Ω and/or a decrease in Ψ leads to a monotonic decrease in its length. An increase in $\varkappa$ from zero to roughly four causes a linear decrease in the relative length of the zone of longitudinal recirculation by 10-15% compared to axisymmetric flow without the jet ($\varkappa = 0$) with the same parameters Ω and Ψ. A further increase in $\varkappa$ has a slight adverse effect. An increase in σ reduces the dependence of the relative length of the longitudinal recirculation zone on the parameter $\varkappa$.

A significant feature of the above flow is the formation of circulation in planes perpendicular to the main flow direction (see Fig. 2d). Its intensity can be approximately characterized by the absolute value of the dimensionless velocity v^3/U^0 of flow through the boundary $x^3 = 0$ (henceforth w_*). The calculations showed that the greater the initial twisting of the flow from the swirlers, the greater the intensity of the transverse circulation. The effect of the parameter Ψ on w_* is characterized by the presence of a maximum of w_* in the range Ψ = 0.3-0.4 (Fig. 3). The effect of $\varkappa$ on the intensity of the transverse circulation is substantial: when $\varkappa = 0$, no transverse circulation is seen; an increase in $\varkappa$ increases w_*. For the investigated range of flow parameters, the maximum value of w_* is reached at $\varkappa \approx 10$. A further increase in $\varkappa$ has no significant effect on w_*. It should be noted that the value of w_* at $\varkappa = 4$ is usually 60-80% of the value of w_* at $\varkappa = 10$. The maximum w_* is reached at σ = 1.3-1.4. With motion of this value in either direction, w_* decreases.

The characteristic rate of mass exchange of the jet system with the main flow from the swirlers can be the rate of decrease in the concentration γ downstream along the jet axis. The calculations revealed an exponential character to this decrease and showed that it is affected mainly by the degree of initial twist of the flow from the swirlers η and the parameter $\varkappa$. An increase in the degree of blockage of the channel Ψ leads to some increase in the counterflow rate in the longitudinal recirculation zone, which in turn decreases the concentration range of the jet. However, this effect is significant only at low values of $\varkappa$. The effect of σ is also manifest at low values of $\varkappa$, but to a lesser degree than in the case of the effect of Ψ. The calculated data for the concentration γ on the jet axis are satisfactorily described by the relation

$$\gamma/\gamma_c = \exp\left\{-6.75(\eta + 0.74)\left(\frac{1 + 0.9\Psi}{\varkappa} + 0.11\right)\frac{x^1}{H}\right\},$$

which is valid for the investigated ranges of the flow parameters.

The data obtained on the flow structure and mass exchange characteristics are supported by experimental data. In particular, the results of visual observations indicate the existence of intensive transverse circulation. Figure 4 shows calculated and experimental data on the change in the concentration of the scalar substance along the jet axis. The agreement is satisfactory.

In turning from the model problem to actual conditions, it should be emphasized that, thanks to the presence of transverse circulation, heat and the active centers are rapidly transferred from the region of longitudinal recirculation to the combustion front at the boundary of the jet, which ensures normal conditions for flame stabilization. On the other hand, intensive transverse mixing, together with a reduction in the length of the longitudinal recirculation zone, leads to rapid equalization of hydrodynamic and temperature fields along the flow.

NOTATION

x^i, cartesian coordinates; v^j, component of the velocity vector in the x^j direction; p, ratio of pressure to constant density; τ^{ij}, components of the turbulent stress tensor; t, time; H, R, height and mean radius of annular channel; h, height of annular surface; s, spacing between jets; r, initial radius of jet; ε, scalar eddy viscosity; L, mixing length; γ, scalar substance; γ_c, value of γ at mouth of jet; U_0, value of longitudinal velocity v^1 at swirler outlet; V_0, value of transverse velocity v^2 at swirler outlet; Ω, angle of initial twist of flow from swirlers; η, degree of initial twist of flow from swirlers; Ψ, degree of blockage of annular channel; U_c, jet discharge velocity; $\varkappa$, relative jet discharge velocity; σ, relative spacing between jets; w_*, intensity of transverse circulation; δ^{ij}, Kronecker delta; ξ^i, transformed coordinates; α^i, coordinate transformation parameter; $\Delta\xi^i$, grid interval; Δt, time interval; $\nu^i = a^i/\Delta\xi^i$; $\lambda^i = \nu^i \Delta t$; E_p^i, difference operator of displacement along coordinate ξ^i by $p\Delta\xi^i$; I, identity operator; $\mu^i = E^i_{i/2} - E^i_{-i/2}$; $\nabla^i = I - E^i_{-i}$; $\Delta^i = E^i_i - I$; δ, asymmetrical unit function; $\bar{\gamma} = \gamma/\gamma_c$; T, flow temperature; T_*, flow temperature at swirler outlet; T_c, temperature at jet mouth; $\bar{\Theta} = (T - T_*)/(T_c - T_*)$; $\bar{x}^i = x^i/H$.

LITERATURE CITED

1. A. L. Dorfman and V. A. Maev, "Numerical study of the interaction of isothermally oppositely twisted flows in an annular channel," Inzh.-Fiz. Zh., 41, No. 4, 674-677 (1981).
2. F. C. Lockwood, "The modeling of turbulent, premixed, and diffusion combustion in the computation of engineering flows," Combust. Flame, 29, No. 2, 111-122 (1977).
3. M. Abou Ellail, A. D. Gosman, and F. C. Lockwood, "Description and validation of three-dimensional procedure for combustion chamber flows," J. Energy, 2, No. 2, 71-80 (1978).
4. J. O. Hinze, Turbulence, McGraw-Hill (1975).
5. O. M. Belotserkovskii, V. A. Gushchin, and V. V. Shchennikov, "Division method applied to the solution of problems of the dynamics of a viscous fluid," Zh. Vychisl. Mat. Mat. Fiz., 15, No. 1, 197-207 (1975).
6. F. H. Harlow and C. W. Hirt, "Recent extensions to Eulerian methods for numerical fluid dynamics," Zh. Vychisl. Mat. Mat. Fiz., No. 3, 656-672 (1972).
7. A. L. Dorfman, "Explicit division scheme with application to a problem of the spatial interaction of a jet of a viscous incompressible liquid in a channel," Chislennye Metody Mekhaniki Sploshnoi Sredy (Novosibirsk), 9, No. 4, 57-67 (1978).
8. A. L. Dorfman, "Solution of equations of the dynamics of a viscous fluid in a curvilinear nonorthogonal coordinate system," Chislennye Metody Mekhaniki Sploshnoi Sredy, 11, No. 6, 79-89 (1980).
9. R. W. McCormick, "Numerical solution of the interaction of a shock wave with a laminar boundary layer," Lect. Notes Phys., 8, 151-163 (1971).